Chemical Science

ROYAL SOCIETY OF CHEMISTRY

EDGE ARTICLE

View Article Online
View Journal | View Issue

Cite this: *Chem. Sci.*, 2024, **15**, 3323

All publication charges for this article have been paid for by the Royal Society of Chemistry

Received 27th November 2023
Accepted 22nd January 2024

DOI: 10.1039/d3sc06331c

rsc.li/chemical-science

Precise synthesis of BN embedded perylene diimide oligomers for fast-charging and long-life potassium–organic batteries†

Guangwei Shao,‡[ab] Hang Liu,‡[ab] Li Chen,[a] Mingliang Wu,[a] Dongxue Wang, *[ab] Di Wu *[ab] and Jianlong Xia *[abc]

Replacing the C=C bond with an isoelectronic BN unit is an effective strategy to tune the optoelectronic properties of polycyclic aromatic hydrocarbons (PAHs). However, precise control of the BN orientations in large PAH systems is still a synthetic challenge. Herein, we demonstrate a facile approach for the synthesis of BN embedded perylene diimide (PDI) nanoribbons, and the polarization orientations of the BN unit were precisely regulated in the two PDI trimers. These BN doped PDI oligomers show great potential as organic cathodes for potassium-ion batteries (PIBs). In particular, ***trans*-PTCDI3BN** exhibits great improvement in voltage potential, reversible capacities (*ca.* 130 mA h g^{-1}), superior rate performance (19 s to 69% of the maximum capacity) and ultralong cyclic stability (nearly no capacity decay over 30 000 cycles), which are among those of state-of-the-art organic-based cathodes. Our synthetic approach stands as an effective way to access large PAHs with precisely controlled BN orientations, and the BN doping strategy provides useful insight into the development of organic electrode materials for secondary batteries.

Introduction

Perylene diimide (PDI) is a versatile building block for the construction of novel functional materials for organic electronics.[1–7] In the past few decades, numerous tailor-made PDI derivatives have been developed for application in electronic devices,[8–13] sensors,[14–17] and energy storage.[18–21] Due to the presence of multiple redox-active carbonyl groups, as well as the merits including but not limited to flexible structure design, low-cost production, excellent stability and environmental friendliness, PDI derivatives have been widely used in almost all kinds of rechargeable ion batteries.[22–25] In terms of material diversity and tunable redox properties, PDI-based electrodes show great potential for application in potassium-ion batteries (PIBs),[26] which have recently been proposed as an alternative to lithium-ion batteries owing to the earth-abundant and widely distributed potassium resources.[27–30] One of the main challenges in the development of PDI-based electrodes is the low electron conductivity of organic materials. Continuous efforts have been devoted to improving the performance of PDI-based energy storage devices;[28,31–36] the construction of oligomers and/or hybrids with extended π-conjugation and an increased number of redox-active sites has been proved to be a robust strategy to obtain high-performance PDI-based electrodes.[22] The enlarged π conjugation can significantly improve the electron conductivity, and the definite chemical structures of PDI oligomers/hybrids can avoid batch-to-batch variations and reduce the use of redox-inactive linkers and side chains in comparison with their polymer counterparts.[37,38] Very recently, Nuckolls and co-workers demonstrated the iterative synthesis of helical PDI nanoribbons; the longest oligomer with six PDI units displayed remarkable cathode performance in lithium batteries, with both high electrical conductivity and high ionic diffusivity.[39] However, the synthetic route toward oligomers with increasing length is somewhat cumbersome and expensive, which hinders further application of this PDI hexamer.

Heteroatom doping is a powerful strategy for tuning the electronic properties of carbon-based materials toward improved electrochemical storage performance; the boron (B) and nitrogen (N) co-doping approach has achieved great success in the development of carbonaceous electrodes.[40–42] And it has also been well established that the substitution of C=C bonds with BN units endows the resultant BN embedded polycyclic aromatic hydrocarbons (PAHs) with similar structural features but with divergent optoelectronic properties.[43–50] We speculated that the use of the B and N co-doping strategy would provide an alternative way for tuning the electrochemical properties of PDI oligomers, besides extending the π conjugation through increasing PDI

[a]*State Key Laboratory of Advanced Technology for Materials Synthesis and Processing, Center of Smart Materials and Devices, Wuhan University of Technology, Wuhan 430070, China. E-mail: chemwd@whut.edu.cn*

[b]*School of Chemistry, Chemical Engineering and Life Science, Wuhan University of Technology, Wuhan 430070, China. E-mail: wangdongxue@whut.edu.cn*

[c]*International School of Materials Science and Engineering, Wuhan University of Technology, Wuhan 430070, China. E-mail: jlxia@whut.edu.cn*

† Electronic supplementary information (ESI) available. See DOI: https://doi.org/10.1039/d3sc06331c

‡ These authors contributed equally to this work.

units with tremendous synthetic efforts. Although the synthetic routes of BN doped PAHs have been well documented, a particular challenge is the precise control of the polarization orientations of BN units in BN-embedded PDI derivatives.[48]

Herein, to prove our hypothesis, a BN bridged PDI dimer **PDI2BN** and a pair of trimers ***trans***- and ***cis***-**PDI3BN** with different BN orientations were designed and precisely synthesized. It is worth noting that the direct bromination of the commercially available PDI monomer usually yields a regioisomeric mixture of 1,7- and 1,6-dibrominated PDI precursors. Although the regioisomeric mixtures of dibrominated PDI intermediates were elaborately used to reduce synthetic efforts in Nuckolls' iterative synthesis of helical PDI nanoribbons,[39] the use of a mixture of 1,7- and 1,6-dibrominated PDI as a starting material gives a mixture of ***trans***- and **cis-PDI3BN**, which could not be separated by column chromatography and crystallization methods. By using a synthetic strategy recently developed in our lab, the regiochemically pure 1,6-di(substituted) PDI precursor can be easily accessed.[51] With these key building blocks in hand, ***trans***- and ***cis***-**PDI3BN** can be separately synthesized. In comparison with the corresponding vinylene bridged counterparts, the photophysical and electronic properties of the PDI oligomers were pronouncedly tuned by the introduction of BN units. The development of PDI-based PIBs lags behind that of other counterparts in terms of understanding the structure–property–performance relationships.[52] The first example of a PDI derivative (3,4,9,10-perylene-tetracarboxylic dianhydride) based PIB cathode with a decent reversible capacity was reported in 2015; however, the potassium storage suffered from poor cyclability.[53] To investigate the electrochemical storage performance of these BN co-doped PDI oligomers, the dealkylated oligomers **PTCDI2BN**, ***trans***- and ***cis***-**PTCDI3BN** (Scheme 1) were prepared, and they all show more superior performance than the vinylene bridged PDI dimer (**PTCDI2**) when employed as the cathode in potassium batteries. The rate performance and cycle stability of the two trimers are among the top class of carbonyl-based potassium batteries, while ***trans***-**PTCDI3BN** shows certain superiority compared with the *cis*-isomer, illustrating the vital role of BN orientation in the performance of organic batteries (Scheme 1).

Results and discussion

As shown in Scheme 2, the synthesis of **PDI2BN** commences with the preparation of **PDI2NH** by reacting 1-Br-PDI **1**[54,55] with 1-NH_2-PDI **2**[56,57] *via* a Buchwald–Hartwig coupling reaction.[58] Subsequently, borylation of **PDI2NH** by treatment with BCl_3, Et_3N affords **PDI2BN** in a yield of 76%. The trimers ***trans***- and ***cis***-**PDI3BN** were synthesized based on the same sequence using the regiochemically pure 1,7- and 1,6-di(substituted) PDI precursors **3** and **4** as staring materials, respectively (Scheme 2). The corresponding dealkylated oligomers **PTCDI2BN**, ***trans***- and ***cis***-**PTCDI3BN** are prepared by vacuum thermolysis at 400 °C (Scheme S7–S9†).[39] The weight loss percentage of these PTCDI oligomers was approximately 48% at 400 °C in thermogravimetric analysis (Fig. S21†), which aligned with the soluble alkyl chain content. And as shown in Fig. S22,† vibrational modes of alkyl chains disappeared in the PTCDI oligomers, accompanied by the appearance of new signals identified as those of N–H stretching vibration. These results indicated that PTCDI oligomers were successfully synthesized. The vinylene bridged PDI dimer **PDI2** and **PTCDI2** (Scheme S10†) were synthesized for comparison following the method described in the literature.[28,59,60] The chemical structures of all new compounds were well characterized by ^{1}H NMR, ^{13}C NMR and HRMS and the synthetic details are illustrated in the ESI.†

The photophysical properties of these BN embedded oligomers were examined by using the ultraviolet-visible (UV-vis) absorption spectra and fluorescence spectra (Fig. 1 and Table 1). As shown in Fig. 1a, on comparing with that of **PDI2**, the absorption band of **PDI2BN** in the 350–425 nm range is almost vanished, which is the characteristic absorption of vinylene bridged **PDI2**.[60–62] Similarly, the characteristic absorption of ***trans***- and ***cis***-**PDI3BN** also disappeared in comparison with vinylene bridged PDI3 (Fig. S1†).[60] ***trans***- and ***cis***-**PDI3BN** showcase a bathochromic-shift of around 20 nm and increased absorption coefficient compared to that of **PDI2BN**, demonstrating the effect of extended conjugation. Furthermore, the different BN orientations in **PDI3BN** lead to distinct fine structures in the absorption spectra, and the *cis*-isomer shows an absorption peak and shoulder at 385 and 609 nm, which may be ascribed to the different dipole–dipole

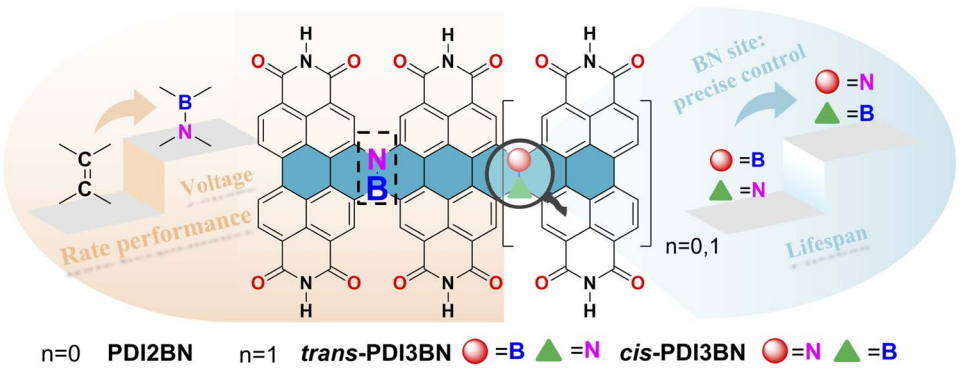

Scheme 1 The design strategy of BN embedded PDI oligomers for high performance PIBs; the structure highlights the effect of BN orientation and the length of conjugation.

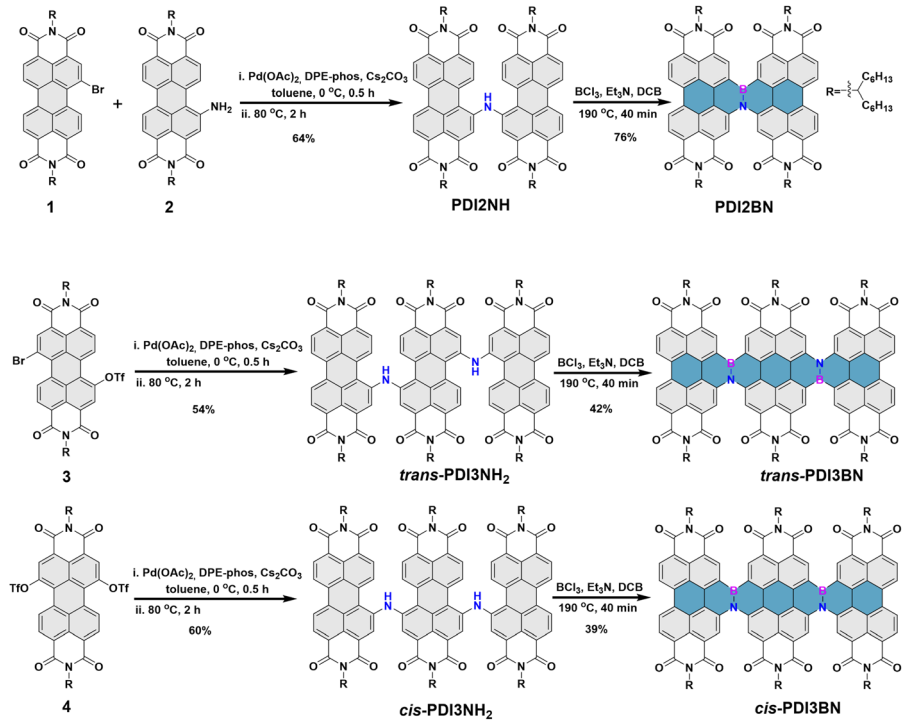

Scheme 2 The synthetic routes of (a) PDI2BN, (b) *trans*-PDI3BN and (c) *cis*-PDI3BN.

interactions of BN units.[48,49] All the three BN embedded PDI oligomers exhibit slightly red-shifted fluorescence compared to vinylene bridged **PDI2** (Fig. 1b) with decreases in fluorescence quantum yields (Table S1†), which are consistent with that of the reported BN embedded PDI.[49] The redox properties of BN embedded oligomers were examined by cyclic voltammetry (CV). All compounds exhibit multiple reduction waves at a given potential (Fig. S2†), which is similar to the reported B–N embedded PDI.[49] The overlapped CV curves of the five cycles of scan and intensified redox peaks with the increase of scanning rates were also observed, demonstrating the splendid reversibility of these oligomers (Fig. S2†).[63–65] The BN doping exerts meagre influence on the energy levels of **PDI2BN** in comparison to **PDI2** (Table 1). In the case of ***trans*-PDI3BN** and ***cis*-PDI3BN**, the orientations of BN units obviously adjust the highest occupied molecular orbital (HOMO) energy level, while the impact on the lowest unoccupied molecular orbital (LUMO) energy level is negligible (Table 1).[49,50]

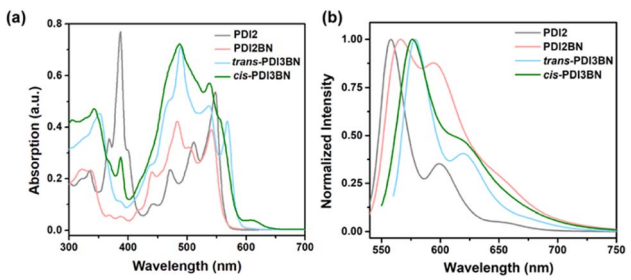

Fig. 1 (a) UV-vis absorption spectra of PDI2, PDI2BN, *trans*-PDI3BN and *cis*-PDI3BN in chloroform (5×10^{-6} M); (b) normalized fluorescence spectra of PDI2, PDI2BN, *trans*- and *cis*-PDI3BN in chloroform (5×10^{-6} M).

Due to the notable redox characteristics of these BN bridged PDI oligomers, they were tested as electrode materials in PIBs.

Table 1 Photophysical and electrochemical parameters of BN embedded oligomers

Compounds	λ_{abs}[a] (nm)	$\varepsilon \times 10^{-5}$ (M^{-1} cm^{-1})	E_{LUMO}[b] (eV)	E_{HOMO}[b] (eV)	E_g[c] (eV)
PDI2	547	1.04	−3.78	−5.97	2.19
PDI2BN	482	0.82	−3.75	−5.93	2.18
***trans*-PDI3BN**	489	1.41	−3.79	−5.90	2.11
***cis*-PDI3BN**	486	1.42	−3.77	−5.72	1.95

[a] λ_{abs} maxima were measured in the $CHCl_3$ solutions of a concentration of 5.0×10^{-6} M. [b] The E_{LUMO} was calculated by using the following equation: $E_{LUMO} = -(E_{red}^{oneset} - E_{Fc} + 4.8)$ eV, where the first reduction potential was measured by CV and E_{Fc} was the half-wave potential of ferrocene. The E_{HOMO} was calculated by using the following equation: $E_{HOMO} = -E_g + E_{LUMO}$ eV. [c] The optical bandgap was estimated from the onset positions of their absorption spectra and calculated by using the equation: $E_g = 1240/\lambda_{onset}$.

The energy storage performances of these PTCDI oligomers were systematically measured in coin cells with potassium metal as the counter electrode and 1 M KPF_6 in ethylene glycol dimethyl ether (DME) as the electrolyte. As shown in Fig. 2a, the cyclic voltammograms (CVs) of the initial three cycles for **PTCDI2BN** are nearly superimposed on each other, while **PTCDI2** shows two irreversible reduction peaks during the initial cathodic scan, implying an irreversible structural transformation.[28] The significant enhancement in reversibility may be related to the changed electron distribution of the carbon plane induced by the heteroelectronic structure afforded by BN doping.[66] Besides, both ***cis***- and ***trans***-**PTCDI3BN** display similar redox behaviors, but obviously extended CV area when compared with **PTCDI2BN**, indicative of their enhanced potassium storage capability. Correspondingly, the galvanostatic charge/discharge (GCD) profiles (Fig. 2b) for all samples are well-consistent with the CV results, *i.e.*, **PTCDI2BN**, ***trans***- and ***cis***-**PTCDI3BN** show similar GCD curves, and both trimers can deliver higher reversible capacities of *ca.* 140 mA h g^{-1} compared to dimers (*ca.* 90 mA h g^{-1}). This should highlight that such a high specific capacity is at the forefront of all carbonyl cathodes for PIBs.[27,31,35,53,67–69] These additional capacities may be rooted in heteroatom substituents in the carbon plane, which changes the surface-chemical properties and enhances the electrochemical adsorption of K^+-ions, further leading to an improved capacity.[41,70] Besides, BN embedded **PTCDI2BN** also shows a *ca.* 0.2 V higher plateau than **PTCDI2** (Fig. 2c and S23†), which can potentially increase the operating voltage of these BN derivative-based full PIBs. It has been shown that a higher redox potential is normally obtained by introducing inactive electron-withdrawing groups, which obviously damages the reversible capacities.[71] Moreover, the balance between stabilizing redox-potential and increasing π-conjugation is always a dilemma since the average voltage would inevitably decrease with an increased π-conjugation degree.[71–74] This dilemma can be effectively circumvented through precise regulation of the polarization orientations of BN units in ***trans***- and ***cis***-**PTCDI3BN**. As displayed in Fig. S23,† a rather low voltage-loss of *ca.* 2.79% is obtained in ***trans***-**PTCDI3BN** (2.09 V *vs.* 2.15 V for **PTCDI2BN**), and a much higher one of *ca.* 12.56% occurred in ***cis***-**PTCDI3BN** (1.88 V *vs.* 2.15 V for **PTCDI2BN**). More particularly, both ***trans***- and ***cis***-**PTCDI3BN** demonstrated remarkable smaller overpotentials of *ca.* 0.02 V than **PTCDI2BN** (Fig. 2d and S24†), implying their better kinetic properties. In summary, BN co-doped PDI oligomers show unique superiorities as follows: (1) heteroelectronic BN linkers can change the electron distributions of the carbon plane, contributing to remarkable improvement in redox potentials of **PTCDI**

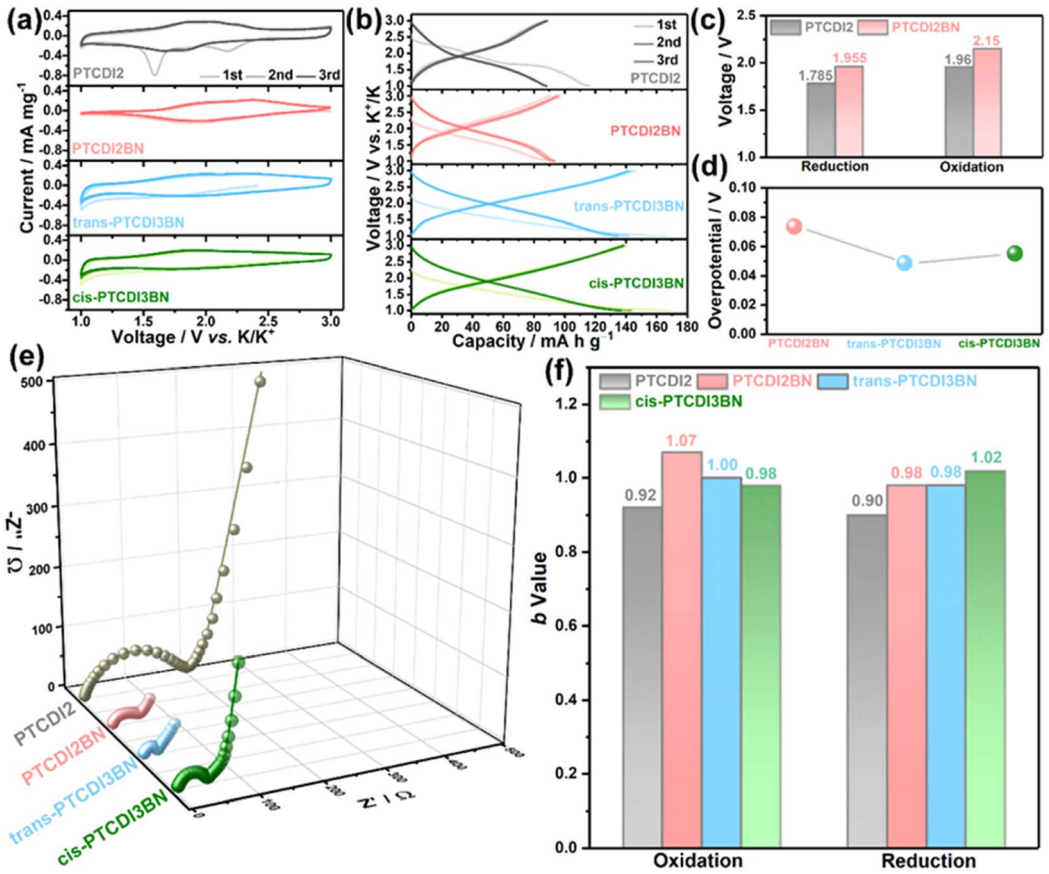

Fig. 2 (a) CV curves at a scan rate of 2 mV s^{-1} and (b) GCD splines at 500 mA g^{-1} during the initial three cycles for **PTCDI** oligomers. (c) The average oxidation and reduction potential comparison picture of **PTCDI2** and **PTCDI2BN**. (d) Overpotential image of BN embedded **PTCDI** derivatives. (e) Nyquist plots and its simulation lines at the third cycle and (f) the histogram for the *b*-value of **PTCDI** oligomers.

derivatives; (2) an increased number of BN linkers offer additional K^+ storage sites, and improve the charge diffusion capability in bulk BN co-doped **PTCDI** trimers; (3) precise control of BN units in PDI trimers as ***trans*-PTCDI3BN** can effectively reduce voltage loss even with increased π-conjugation. Fig. 2e demonstrates that the charge transfer resistance (R_{ct}) is significantly reduced with the increase of BN linkers (Fig. S25†), and ***trans*-PTCDI3BN** displayed the smallest R_{ct} value, reflecting its fastest reaction kinetics. Detailed fitted R_{ct} values are presented in Table S2.† Furthermore, a series of rectangle-like CV curves with recognized redox peaks (Fig. S26†) are observed at various scan rates from 0.5 to 10 mV s^{-1}, suggestive of co-managed Faradaic and non-Faradaic behaviors during repeated K^+ release/storage in these four **PTCDI** oligomers. According to the power law between measured current (i) and sweep rates (v) shown in eqn S1 and S2,† **PTCDI2BN**, ***trans*-** and ***cis*-PTCDI3BN** demonstrate a higher b-value compared to **PTCDI2**, implying that BN co-doping is beneficial to increase the contribution from pseudocapacitance (Fig. 2f and S27†).

Encouraged by the improvement in K^+ storage and transfer capability through BN co-doping, we further assessed their rate performance. As shown in Fig. 3a, all the BN doped **PTCDI** oligomers displayed apparent superiority in high-rate capability compared to **PTCDI2**, and both ***trans*-** and ***cis*-PTCDI3BN** exhibit enhanced reversible capacities and capacity retention at various current densities. Specifically, ***trans*-PTCDI3BN** exhibits a capacity response of *ca.* 135.2 mA h g^{-1} at a current density of 0.5 A g^{-1}, and 69% of it can be retained even at a high rate of 20 A g^{-1}, suggestive of its excellent structural stability. Moreover, GCD curves collected at various current densities (Fig. 3b) reveal the electrode polarization order to be ***trans*-PTCDI3BN** < ***cis*-PTCDI3BN** < **PTCDI2BN** < **PTCDI2**, which is in accordance with EIS results and indicates the outstanding high-rate endurance of both ***trans*-** and ***cis*-PTCDI3BN** again. Furthermore, all three BN embedded **PTCDI** oligomers outperform most of the state-of-the-art carbonyl cathodes for PIBs (Fig. 3c).[28,33,35,36,38,53,75–82] Besides boosting the rate performance, the extended conjugated structure of **PTCDI3BN** also contributes to remarkable improvement in cyclic durability, which was evaluated at high current densities of 10 A g^{-1} and 20 A g^{-1}, respectively (Fig. 3d and e). Moreover, ***trans*-PTCDI3BN** exhibits the best cyclability among these four **PTCDI** oligomers, followed by by ***cis*-PTCDI3BN**. In detail, there is nearly no capacity fading in the ***trans*-PTCDI3BN** cathode even after 13 000 cycles at 10 A g^{-1} and 30 000 cycles at 20 A g^{-1}. Furthermore, the ***cis*-PTCDI3BN** cathode exhibits a high reversible capacity of 78.4 mA h g^{-1} over 9000 cycles at 10 A g^{-1}, and retained 91% of its initial value. Even after 20 000 cycles, a capacity retention of 85% can still be achieved. It should be highlighted that such an ultra-long lifespan over 30 000 cycles with a capacity retention of nearly 100% is among the best ones in state-of-the-art potassium storage.

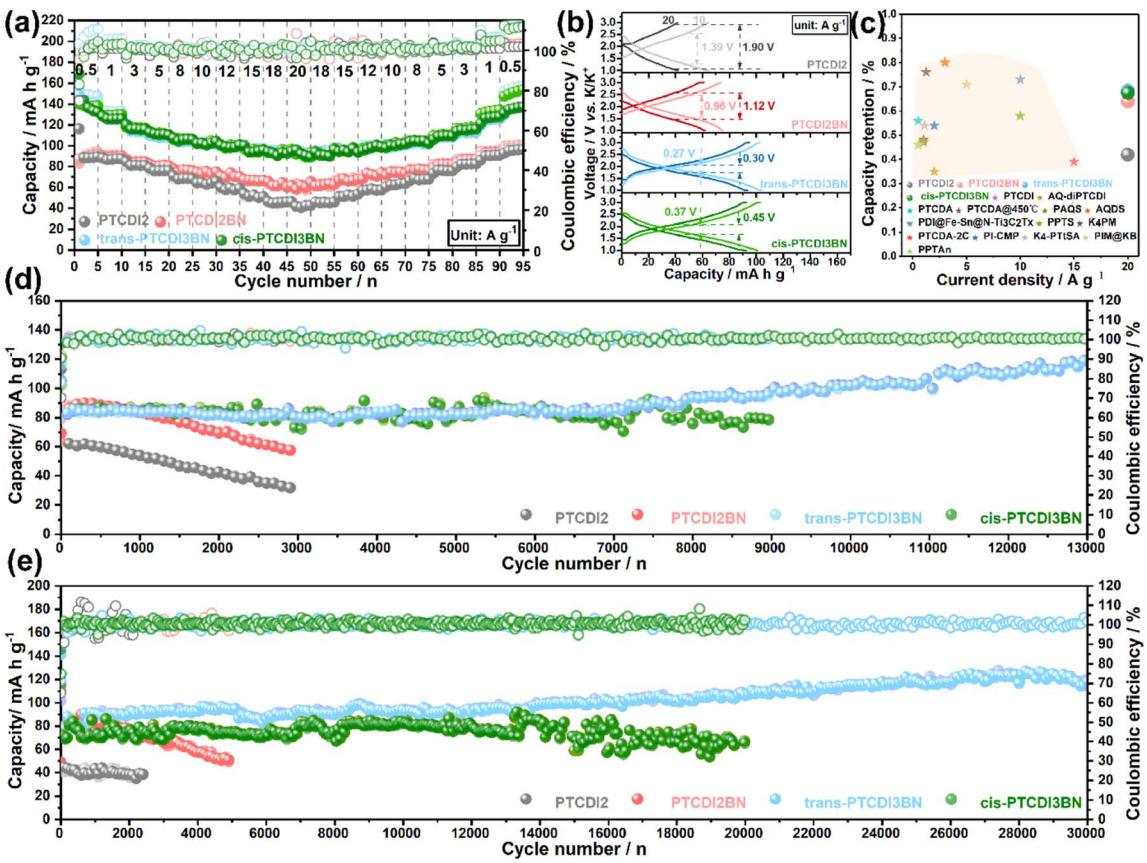

Fig. 3 (a) The cycle performance at different current densities and (b) ohmic polarization at the selected current density for **PTCDI** oligomers. (c) Comparison of the capacity retention among various reported OEMs. Cycle stability of **PTCDI** oligomers at (d) 10 A g^{-1} and (e) 20 A g^{-1}.

Conclusions

In conclusion, a two-step synthetic route toward boron and nitrogen co-doped PDI oligomers with precisely controlled BN orientations was developed. The optoelectronic properties of the obtained **PDI2BN** and ***trans***- and ***cis***-**PDI3BN** were investigated. The introduction of BN units causes pronounced changes in the absorption and emission characteristics as compared with those of the vinylene bridged PDI oligomers. The difference in LUMO energy levels of ***trans***- and ***cis***-**PDI3BN** reveals the influence of BN orientations. Furthermore, the successful application of dealkylated BN embedded PDI oligomers in PIBs strongly verifies the superiority of the B, N co-doping design strategy. Potassium batteries using **PTCDI2BN** and ***trans***- and ***cis***-**PTCDI3BN** as cathodes show excellent rate performance and cycle stability. Among them, ***trans***-**PTCDI3BN** shows remarkable superiority with ultrafast-charging capacity and a capacity retention of 100% over 30 000 cycles, which displays great potential for practical application in PIBs. The synthetic route developed here offers an applicable method to access BN embedded PDI derivatives, and the B, N co-doping strategy provides an effective way for tuning the electrochemical performance of organic electrodes for potassium batteries with excellent rate performance and cycle stability.

Data availability

All experimental details and data supporting the findings of this study are available within the paper and its ESI.† And original data can be obtained by contacting the corresponding authors.

Author contributions

G. Shao and H. Liu conducted the experiments and finished the manuscript. L. Chen and M. Wu provided assistance for the investigation. D. Wang, D. Wu. and J. Xia conducted the project administration, and writing as well as editing of this manuscript.

Conflicts of interest

There are no conflicts to declare.

Acknowledgements

This work was supported by the National Natural Science Foundation of China (NSFC, 21801201, 51773160, 21975194, 22209127 and 22175134) and Natural Science Foundation of Hubei Province (No. 2023AFA014).

Notes and references

1 F. Würthner, C. Saha-Möller, B. Fimmel, S. Ogi, P. Leowanawat and D. Schmidt, *Chem. Rev.*, 2015, **116**, 962–1052.
2 A. Nowak-Król and F. Würthner, *Org. Chem. Front.*, 2019, **6**, 1272–1318.
3 M. Sun, K. Müllen and M. Yin, *Chem. Soc. Rev.*, 2016, **45**, 1513–1528.
4 E. Krieg, A. Niazov-Elkan, E. Cohen, Y. Tsarfati and B. Rybtchinski, *Acc. Chem. Res.*, 2019, **52**, 2634–2646.
5 Z. Yang and X. Chen, *Acc. Chem. Res.*, 2019, **52**, 1245–1254.
6 C. Schaack, A. Evans, F. Ng, M. Steigerwald and C. Nuckolls, *J. Am. Chem. Soc.*, 2021, **144**, 42–51.
7 W. Jiang and Z. Wang, *J. Am. Chem. Soc.*, 2022, **144**, 14976–14991.
8 G. Zhang, J. Zhao, P. Chow, K. Jiang, J. Zhang, Z. Zhu, J. Zhang, F. Huang and H. Yan, *Chem. Rev.*, 2018, **118**, 3447–3507.
9 P. Cheng, X. Zhao and X. Zhan, *Acc. Mater. Res.*, 2022, **3**, 309–318.
10 X. Zhan, A. Facchetti, S. Barlow, T. Marks, M. Ratner, M. Wasielewski and S. Marder, *Adv. Mater.*, 2011, **23**, 268–284.
11 B. Zhang, G. Lyu, E. Kelly and R. Evans, *Adv. Sci.*, 2022, **9**, 2201160.
12 C. Li and H. Wonneberger, *Adv. Mater.*, 2012, **24**, 613–636.
13 J. Anthony, A. Facchetti, M. Heeney, S. Marder and X. Zhan, *Adv. Mater.*, 2010, **22**, 3876–3892.
14 V. Praveen, B. Vedhanarayanan, A. Mal, R. Mishra and A. Ajayaghosh, *Acc. Chem. Res.*, 2020, **53**, 496–507.
15 P. Singh, A. Hirsch and S. Kumar, *TrAC, Trends Anal. Chem.*, 2021, **138**, 116237.
16 Z. Wang, T. Liu, H. Peng and Y. Fang, *J. Phys. Chem. B*, 2023, **127**, 828–837.
17 S. Chen, M. Zhou, L. Zhu, X. Yang and L. Zang, *Chemosensors*, 2023, **11**, 293.
18 M. Wu and Z. Zhou, *Interdiscip. Mater.*, 2023, **2**, 231–259.
19 J. Russell, V. Posey, J. Gray, R. May, D. Reed, H. Zhang, L. Marbella, M. Steigerwald, Y. Yang, X. Roy, C. Nuckolls and S. Peurifoy, *Nat. Mater.*, 2021, **20**, 1136–1141.
20 L. Zhu, G. Ding, L. Xie, X. Cao, J. Liu, X. Lei and J. Ma, *Chem. Mater.*, 2019, **31**, 8582–8612.
21 H. g. Wang and X. b. Zhang, *Chem. - Eur. J.*, 2018, **24**, 18235–18245.
22 Y. Yu and J. Chen, *Nat. Rev. Chem*, 2020, **4**, 127–142.
23 J. Kim, Y. Kim, J. Yoo, C. Kwon, Y. Ko and K. kang, *Nat. Rev. Chem*, 2023, **8**, 54–70.
24 T. Schon, B. McAllister, P. Li and D. S. Seferos, *Chem. Soc. Rev.*, 2016, **45**, 6345–6404.
25 P. Poizot, J. Gaubicher, S. Renault, L. Dubois, Y. Liang and Y. Yao, *Chem. Rev.*, 2020, **120**, 6490–6557.
26 Y. Feng, Y. Lv, H. Fu, M. Parekh, A. M. Rao, H. Wang, X. Tai, X. Yi, Y. Lin, J. Zhou and B. Lu, *Natl. Sci. Rev.*, 2023, **10**, nwad118.
27 H. Liu, M. Cheng, Z. Tian, L. Cui, D. Wu, D. Wang, L. Zhou and J. Xia, *Adv. Funct. Mater.*, 2023, 2306424.
28 D. Wang, X. You, M. Wu, H. Huang, L. Chen, D. Wu and J. Xia, *ACS Appl. Mater. Interfaces*, 2021, **13**, 16396–16406.
29 H. Wang, F. Liu, R. Yu and J. Wu, *Interdiscip. Mater.*, 2022, **1**, 196–212.
30 Y. Huang, *Interdiscip. Mater.*, 2022, **1**, 323–329.
31 L. Fan, R. Ma, J. Wang, H. Yang and B. Lu, *Adv. Mater.*, 2018, **30**, 1805486.

32 Z. Zhang, Y. Zhu, M. Yu, Y. Jiao and Y. Huang, *Nat. Commun.*, 2022, **13**, 6489.
33 Z. Tong, S. Tian, H. Wang, D. Shen, R. Yang and C. Lee, *Adv. Funct. Mater.*, 2019, **30**, 1907656.
34 J. Ge, X. Yi, L. Fan and B. Lu, *J. Energy Chem.*, 2021, **57**, 28–33.
35 J. Zheng, X. Liu, W. Li, W. Li, X. Feng and W. Chen, *Nano Res.*, 2023, **16**, 9538–9545.
36 P. Han, F. Liu, Y. Zhang, Y. Wang, G. Qin, L. Hou and C. Yuan, *Angew. Chem., Int. Ed.*, 2021, **60**, 23596–23601.
37 M. Bhosale, S. Chae, J. Kim and J. Choi, *J. Mater. Chem. A*, 2018, **6**, 19885–19911.
38 Y. Hu, W. Tang, Q. Yu, X. Wang, W. Liu, J. Hu and C. Fan, *Adv. Funct. Mater.*, 2020, **30**, 2000675.
39 Z. Jin, Q. Cheng, S. Bao, R. Zhang, A. M. Evans, F. Ng, Y. Xu, M. Steigerwald, A. McDermott, Y. Yang and C. Nuckolls, *J. Am. Chem. Soc.*, 2022, **144**, 13973−13980.
40 C. Sathish, G. Kothandam, P. Selvarajan, Z. Lei, J. Lee, J. Qu, A. Al-Muhtaseb, X. Yu, M. Breese, R. Zheng, J. Yi and A. Vinu, *Adv. Sci.*, 2022, **9**, 2105603.
41 X. Lian, J. Zhou, Y. You, Z. Tian, Y. Yi, J. Choi, M. Rümmeli and J. Sun, *Adv. Funct. Mater.*, 2022, **32**, 2109969.
42 M. Wang, Y. Yang, Z. Yang, L. Gu, Q. Chen and Y. Yu, *Adv. Sci.*, 2017, **4**, 1600468.
43 X. Chen, D. Tan and D. Yang, *J. Mater. Chem. C*, 2022, **10**, 13499–13532.
44 X. Wang, J. Wang and J. Pei, *Chem. - Eur. J.*, 2014, **21**, 3528–3539.
45 J. Wang and J. Pei, *Chin. Chem. Lett.*, 2016, **27**, 1139–1146.
46 H. Helten, *Chem. - Eur. J.*, 2016, **22**, 12972–12982.
47 T. Hatakeyama, S. Hashimoto, S. Seki and M. Nakamura, *J. Am. Chem. Soc.*, 2011, **133**, 18614–18617.
48 P. Zhang, J. Zeng, F. Zhuang, K. Zhao, Z. Sun, Z. Yao, Y. Lu, X. Wang, J. Wang and J. Pei, *Angew. Chem., Int. Ed.*, 2021, **60**, 23313–23319.
49 K. Zhao, Z. Yao, Z. Wang, J. Zeng, L. Ding, M. Xiong, J. Wang and J. Pei, *J. Am. Chem. Soc.*, 2022, **144**, 3091–3098.
50 Y. Chen, W. Chen, Y. Qiao, X. Lu and G. Zhou, *Angew. Chem., Int. Ed.*, 2020, **59**, 7122–7130.
51 G. Shao, M. Wu, X. Wang, J. Zhao, X. You, D. Wu and J. Xia, *J. Org. Chem.*, 2022, **87**, 14825–14832.
52 L. Li, Y. Yin, J. Hei, X. Wan, M. Li and Y. Cui, *Small*, 2021, **17**, 2005752.
53 Y. Chen, W. Luo, M. Carter, L. Zhou, J. Dai, K. Fu, S. Lacey, T. Li, J. Wan, X. Han, Y. Bao and L. Hu, *Nano Energy*, 2015, **18**, 205–211.
54 Y. Guo, Y. Li, O. Awartani, H. Han, J. Zhao, H. Ade, H. Yan and D. Zhao, *Adv. Mater.*, 2017, **29**, 1700309.
55 Z. Luo, F. Wu, T. Zhang, X. Zeng, Y. Xiao, T. Liu, C. Zhong, X. Lu, L. Zhu, S. Yang and C. Yang, *Angew. Chem., Int. Ed.*, 2019, **58**, 8520–8525.
56 Z. Luo, K. Wu, Y. Zhao, B. Qiu, Y. Li and C. Yang, *Dyes Pigm.*, 2019, **163**, 356–362.
57 A. Goujon, L. Rocard, T. Cauchy and P. Hudhomme, *J. Org. Chem.*, 2020, **85**, 7218–7224.
58 X. Wang, F. Zhuang, X. Zhou, D. Yang, J. Wang and J. Pei, *J. Mater. Chem. C*, 2014, **2**, 8152–8161.
59 Y. Li, C. Wang, L. Cheng, S. Di Motta, F. Negri and Z. Wang, *Org. Lett.*, 2012, **14**, 5278–5281.
60 Y. Zhong, B. Kumar, S. Oh, M. T. Trinh, Y. Wu, K. Elbert, P. Li, X. Zhu, S. Xiao, F. Ng, M. L. Steigerwald and C. Nuckolls, *J. Am. Chem. Soc.*, 2014, **136**, 8122–8130.
61 Y. Zhong, M. Trinh, R. Chen, W. Wang, P. Khlyabich, B. Kumar, Q. Xu, C. Nam, M. Sfeir, C. Black, M. Steigerwald, Y. Loo, S. Xiao, F. Ng, X. Zhu and C. Nuckolls, *J. Am. Chem. Soc.*, 2014, **136**, 15215–15221.
62 M. Wu, J. Yi, L. Chen, G. He, F. Chen, M. Sfeir and J. Xia, *ACS Appl. Mater. Interfaces*, 2018, **10**, 27894–27901.
63 J. Tan, G. Zhang, C. Ge, J. Liu, L. Zhou, C. Liu, X. Gao, A. Narita, Y. Zou and Y. Hu, *Org. Lett.*, 2022, **24**, 2414–2419.
64 S. Zhao, Z. Bian, Z. Liu, Y. Wang, F. Cui, H. g. Wang and G. Zhu, *Adv. Funct. Mater.*, 2022, **32**, 2204539.
65 X. Li, W. Liu, Y. Wang, L. Lv, H. Feng, W. Huang, Y. Sun, W. Xiong and H. Zheng, *Chem. Eng. J.*, 2023, **473**, 145310.
66 D. Chao, C. Zhu, P. Yang, X. Xia, J. Liu, J. Wang, X. Fan, S. V. Savilov, J. Lin, H. Fan and Z. Shen, *Nat. Commun.*, 2016, **7**, 1–8.
67 S. Li, J. Cao, T. Wang, L. Wang, H. Deng, Q. Zhang, Y. Cheng, J. Zhu and B. Lu, *Chem. Eng. J.*, 2022, **431**, 133215.
68 J. Zhao, J. Yang, P. Sun and Y. Xu, *Electrochem. Commun.*, 2018, **86**, 34–37.
69 A. Yu, Q. Pan, M. Zhang, D. Xie and Y. Tang, *Adv. Funct. Mater.*, 2020, **30**, 2001440.
70 X. Chen, P. Ye, H. Wang, H. Huang, Y. Zhong and Y. Hu, *Adv. Funct. Mater.*, 2023, **33**, 2212915.
71 H. Banda, D. Damien, K. Nagarajan, A. Raj, M. Hariharan and M. M. Shaijumon, *Adv. Energy Mater.*, 2017, **7**, 1701316.
72 Y. Lu, Q. Zhang, L. Li, Z. Niu and J. Chen, *Chem*, 2018, **4**, 2786–2813.
73 Z. Song, Y. Qian, M. L. Gordin, D. Tang, T. Xu, M. Otani, H. Zhan, H. Zhou and D. Wang, *Angew. Chem., Int. Ed.*, 2015, **54**, 13947–13951.
74 Z. Tie and Z. Niu, *Angew. Chem., Int. Ed.*, 2020, **59**, 21293–21303.
75 B. Li, J. Zhao, Z. Zhang, C. Zhao, P. Sun, P. Bai, J. Yang, Z. Zhou and Y. Xu, *Adv. Funct. Mater.*, 2018, **29**, 1807137.
76 Q. Pan, Y. Zheng, Z. Tong, L. Shi and Y. Tang, *Angew. Chem., Int. Ed.*, 2021, **60**, 11835–11840.
77 J. Wang, X. Liu, H. Jia, P. Apostol, X. Guo, F. Lucaccioni, X. Zhang, Q. Zhu, C. Morari, J.-F. Gohy and A. Vlad, *ACS Energy Lett.*, 2022, **7**, 668–674.
78 Y. Hu, Y. Gao, L. Fan, Y. Zhang, B. Wang, Z. Qin, J. Zhou and B. Lu, *Adv. Energy Mater.*, 2020, **10**, 2002780.
79 B. Tian, J. Zheng, C. Zhao, C. Liu, C. Su, W. Tang, X. Li and G.-H. Ning, *J. Mater. Chem. A*, 2019, **7**, 9997–10003.
80 C. Zhang, Y. Xu, K. He, Y. Dong, H. Zhao, L. Medenbach, Y. Wu, A. Balducci, T. Hannappel and Y. Lei, *Small*, 2020, **16**, 2002953.
81 L. Fan, Q. Liu, Z. Xu and B. Lu, *ACS Energy Lett.*, 2017, **2**, 1614–1620.
82 M. Tang, Y. Wu, Y. Chen, C. Jiang, S. Zhu, S. Zhuo and C. Wang, *J. Mater. Chem. A*, 2019, **7**, 486–492.